On the evolution of seismogenic faults in the Longmen Shan, eastern Tibet

Huiping Zhang[1]*, Guixi Yi[2], Peizhen Zhang[1], Eric Kirby[3]

[1] *State Key Laboratory of Earthquake Dynamics, Institute of Geology, China Earthquake Administration, Beijing 100029, China*

[2] *Earthquake Administration of Sichuan Province, Chengdu, 610041, China*

[3] *College of Earth, Ocean and Atmospheric Sciences, Oregon State University, Corvallis, Oregon 97331, USA*

* E-mail: huiping@ies.ac.cn (H-p. Zhang)

Abstract: A fundamental debate exists regarding the geometry and depth extent of seismogenic faults in eastern Tibet. Along the Longmen Shan, geologic and seismic reflection data reveal a belt of low to moderate angle thrust faults, some of which may have been activated in devastating earthquakes in 2008 (*M*w ~7.9, Wenchuan) and 2013 (*M*w ~6.6, Lushan). However, geologic and geodetic constraints on these ruptures suggest rupture along relatively high-angle listric reverse faults. Here, we use a combination of focal mechanisms determined from 276 aftershocks (*M*s>4.0) with well-determined waveforms and aftershock distributions from the 2008 event to determine subsurface fault geometry. Our results imply that seismogenic slip occurred along relatively high-angle structures that cross-cut low-angle imbricate faults imaged in reflection seismic data. Thus, we suggest that current geometric models of seismogenic faults may not fully represent the distribution of subsurface seismic hazard along the heavily-populated Sichuan Basin.

Keywords: Longmen Shan; eastern Tibet; seismogenic fault; seismic hazard

1. Introduction

Understanding the distribution of seismic hazard in intracontinental regions is a first-order problem, since relatively low rates of strain accumulation and sparse historic seismicity of these regions pose challenges for evaluation based on both geodetic data and probabilistic approaches (Bilham, 2004). Moreover, in regions that have been subject to multiple periods of orogeny, complex distributions of pre-existing crustal weaknesses present difficulties in the recognition and characterization of active structures. This situation is typically challenging for assessing seismic hazard in Eurasia, because most of the ~200 active faults are distributed along the pre-existing block boundaries and have been reactivated during the Cenozoic (Deng et al., 2007). For example, active thrust faults near the eastern end of the Haiyuan fault in NE Tibet apparently originated as a normal fault in the Oligocene to early Miocene (Wang et al., 2013). Although the general case of fault inversion is rather well-known (e.g., McClay, 1989), distinguishing reactivated structures from newly formed faults with low-magnitude displacement may be challenging.

In eastern Tibet, faults along the Longmen Shan hosted devastating earthquakes in 2008 (Wenchuan, Mw ~7.9) and 2013 (Lushan, Mw ~6.6). These events occurred in a region considered to be of only moderate seismic hazard (P Zhang, 2013) due to slow rates of deformation and strain accumulation (e.g., Gan et al., 2007). Among three strands of the Longmen Shan faults, Beichuan and Pengguan faults ruptured during the 2008 Mw 7.9 Wenchun earthquake

(Figure 1; Fu et al., 2011; Liu-Zeng et al., 2009; Xu et al., 2009; Zhang et al., 2010). Geological context for generating this event has been a hotspot in that it is essential to understand the Cenozoic evolution of the eastern Tibetan Plateau, and it is also a critical target to test the geodynamical models proposed to describe the evolution of the region. Because these events occurred along a fold-and-thrust belt that initially developed in Mesozoic time (Burchfiel et al., 1995; Chen and Wilson, 1996) and was reactivated in the middle Cenozoic (Burchfiel et al., 1995; Richardson et al., 2008; Wang et al., 2012), determining whether these events occurred along pre-existing structures or along newly developed faults is challenging (c.f., Hubbard and Shaw, 2009; Zhang et al., 2010). Therefore, the geometry of the seismogenic Longmen Shan faults responsible for the events is not well constrained and still hotly debated. Geological and numerical modeling observations favor a listric geometry (Feng et al., 2010; Shen et al., 2009; Zhang et al., 2010; Zhu and Zhang, 2010, 2013), however, almost all the geophysical surveys argued for an overthrusting imbricated faults (Hubbard and Shaw, 2009; Jia et al., 2010; Y Li et al., 2010), which are thought obviously responsible for the 2008 *M*w 7.9 earthquake.

Here we present an analysis of aftershocks following the 2008 Wenchuan event; their spatial distribution and focal mechanisms are consistent with rupture along a steep (>40°) fault zone. These results support the notion that at least some seismogenic faults in the Longmen Shan are recently formed and cross-cut the imbricate fold-and-thrusts observed in reflection seismic data.

2. Background: tectonics of the Longmen Shan

The Longmen Shan, a mountain range approximately 500 km long and 30-50 km wide, marks the steep topographic transition from the Sichuan Basin to the eastern Tibetan Plateau (Figure 1) (Clark and Royden, 2000; Kirby et al., 2003). The fault system along the Longmen Shan initially developed during Mesozoic convergence between the North China Block, South China Block and the Songpan-Garze basin (Burchfiel et al., 1995; Chen et al., 1995; Cook et al., 2013; Jia et al., 2006). Shortening and fabric development within the Mesozoic orogen involved emplacement of a series of nappes over foreland strata (Burchfiel et al., 1995; Chen and Wilson, 1996), whereas ductile deformation within the hinterland led to fabric development along the sinistral-oblique Wenchuan-Maowen shear zone (Dirks et al., 1994). Cenozoic deformation was superimposed upon these early fabrics and structures (Burchfiel et al., 1995, 2008). Consequently, deconvolving the history of slip along them is challenging, and significant uncertainty still remains regarding the geometry of active structures and the magnitude of Cenozoic displacement.

At the lithospheric scale, the Longmen Shan is an enigmatic mountain range, with relatively modest shortening (Burchfiel et al., 1995, 2008), but a thick crustal root (Robert et al., 2010a, 2010b). In conjunction with the absence of a foreland basin and limited shortening rates observed geodetically (e.g., Gan et al., 2007; Loveless and Meade, 2011), these observations imply a mode of mountain building that does not lead to a flexural load of the basin (Burchfiel et al., 2008). It has been suggested that flow of the lower crust provides a means to explain these observations (Clark and Royden, 2000; Clark et al., 2005; Kirby et al., 2002; Royden et al., 1997), and this model is consistent with geophysical observations of high conductivity and elevated temperature which suggest low viscosity in middle and lower crust (Bai et al., 2010; Zhao et al., 2012). Not all workers agree, however, as structures observed on seismic reflection profiles (Hubbard and Shaw, 2009; Jia et al., 2006, 2010; Y Li et al., 2010) have been interpreted to represent up to ~50% shortening of the upper crust across the Longmen Shan foothills (Hubbard and Shaw, 2009). An apparent correlation between structural and topographic relief approaching the Longmen Shan led these authors to conclude that brittle shortening through low-angle thrust faulting is closely linked to the production of steep topography.

Against this geodynamic backdrop, the geometry of active faults in the Longmen Shan plays a central role in a current debate over the nature and distribution of seismic hazard. Active convergent and right-lateral deformation along the Longmen Shan is accomplished along series of major faults (Burchfiel et al., 1995, 2008; Densmore et al., 2007; Fu et al., 2011; Kirby et al., 2002), from northwest to southeast, the Wenchuan-Maoxian, Beichuan, and Pengguan faults, and blind range front thrusts (Figure 1) that collectively define an east-vergent imbricate fault system (e.g., Hubbard and Shaw, 2009). Well constrained studies of active faults indicate that the slip rates (both dip-slip and strike-slip) averaged over tens of millennia are around 2 mm/a or less

(Densmore et al., 2007; Zhang et al., 2011), consistent with decadal GPS observations (Chen et al., 2000; Gan et al., 2007; Zhang et al., 2004).

The southeastern two faults of the Longmen Shan fault system ruptured during large to moderate-magnitude reverse events in 2008 and 2013 (Xu et al., 2009, 2013; Zhang et al., 2010; Y Zhang et al., 2013). Along the Beichuan fault, the 2008 Mw 7.9 Wenchuan earthquake was associated with a 240-km-long surface rupture while an additional 72-km-long surface rupture occurred along the Pengguan fault (Figure 1) (Xu et al., 2009). Maximum vertical and horizontal offsets of ~9.0 m and 4.9 m (Liu-Zeng et al., 2009; Zhang et al., 2010), respectively, were measured along the Beichuan fault. A maximum vertical offset of 3.5 m was measured along the Pengguan fault (Liu-Zeng et al., 2009; Xu et al., 2009; Zhang et al., 2010). This earthquake was characterized by pronounced along-strike variations in the magnitude and direction of co-seismic slip (Hao et al., 2009; Liu-Zeng et al., 2009; Xu et al., 2009; Zhang et al., 2010). Between the southern terminus of the rupture, near the cities of Yingxiu and Beichuan, right-lateral slip occurred with a significant component of dip-slip (Feng et al., 2010; Liu-Zeng et al., 2009; Shen et al., 2009; Zhang et al., 2010). North of Beichuan, however, primarily right-lateral strike slip occurred (Feng et al., 2010; Hao et al., 2009; Xu et al., 2009; Zhang et al., 2010).

These variations in co-seismic slip appear to be associated with differences in geometry of the rupture plane. Surface exposures of the surface rupture along the Beichuan fault exhibit dips of 70–80º to the northwest (C Li et al., 2010;

Liu-Zeng et al., 2009; Zhang et al., 2010), in agreement with trench excavations and with a borehole drilled to a depth of ~ 590 m (H Li et al., 2013). Moreover, aftershocks are confined to relatively narrow region, ~15 – 30 km wide, northwest of the Beichuan fault (Zhang et al., 2010) (Figure 1). Far-field coseismic displacements recorded with GPS and InSAR imply that slip occurred a relatively high-angle fault (~45 – 50°) (Feng et al., 2010; Shen et al., 2009). Collectively, the distribution of aftershocks, inversion of geodetic data, and the best-fit seismic moment tensor (~30° fault plane at ~18 km, Wang et al., 2008) all suggest that, near the epicenter area, the coseismic Beichuan fault is a high-angle listric thrust fault that dips ~70° in the shallow crust, but only 30° to 40° below ~15 km depth. The fault presumably roots into a sub-horizontal brittle-ductile transition zone below ~20 km depth (Zhang et al., 2010; Zhu and Zhang, 2010, 2013). Along the northeastern segments of the rupture, aftershock locations and observations of fault scarps indicate that the dip of the near-surface rupture plane is even steeper, approaching 90° (Xu et al., 2009). Likewise, slip inversions of geodetic data by Shen et al. (2009) and Feng et al. (2010) both support a steeper fault geometry along these segments of the Beichuan fault.

These observations, however, contrast with the geometry of fault systems as imaged in the subsurface of the Longmen Shan foreland. Seismic reflection surveys reveal moderately- to shallowly-oriented imbricated faults that are organized in a series of east-vergent fold and thrust systems (Hubbard and Shaw, 2009; Hubbard et al., 2010; Jia et al., 2006, 2010; Y Li et al., 2010). Some have argued that the close coincidence of the surface trace of the 2008 Wenchuan rupture with the mapped trace of the Beichuan and Pengguan faults implies that rupture utilized these moderately to shallowly west-dipping faults (Figures 2a and 2b) (Jia et al., 2010). Seismic data are confined to the foreland of the range, and, thus the geometry of the fault plane is inferred by projection of near surface structures to the hypocentral depth (Figure 2a) (Hubbard and Shaw, 2009; Jia et al., 2010; Y Li et al., 2010). A similar situation occurs along the northern segment of the Beichuan fault (Figure 2b). Here, the trace of the 2008 surface rupture is nearly coincident with mapped, west-dipping thrust faults (Jia et al., 2010; Y Li et al., 2010). These workers suggest that rupture occurred along a plane that dips ~30 – 45° in the shallow crust, but gradually decreases to ~15 – 20° by ~7 km depth (Figure 2b) (Jia et al., 2010).

Similar controversy exists for the 2013 Lushan earthquake (*M* 6.6), which ruptured the frontal fault system in the southern Longmen Shan (Figures 1 and 2). Although aftershocks of this event are also distributed along the Longmen Shan faults (Xu et al., 2013), debate persists regarding the exact fault strand that ruptured (Chen et al., 2013; Li et al., 2014; Xu et al., 2013; Y Zhang et al., 2013). Relocations of the aftershocks show that seismicity is spread along 35 km of the fault length and across 16 km in width, and most of the focal depths lie between 10 and 20 km depth (Fang et al., 2013). Focal depth profiles of the Lushan mainshock and aftershocks show that the coseismic fault planes dip to the northwest, but likely become shallower as a listric thrust fault at depth (Fang et al., 2013). Since field investigations revealed only limited brittle compressive fissures in cement-covered pavement, this earthquake is inferred to have ruptured a blind thrust fault (Xu et al., 2013). Consequently, whether the Pengguan fault (locally known as Shuangshi-Dachuan fault) was responsible or whether slip occurred on one of the faults mapped father east in the foreland is still difficult to determine (Chen et al., 2013; Li et al., 2014; Xu et al., 2013; Y Zhang et al., 2013).

3. Evidence for cross-cutting fault geometry

In order to evaluate the details of fault geometry along the Beichuan fault, we analyzed 276 Ms>4.0 aftershocks with high signal-to-noise ratio waveforms to first obtain focal mechanism solutions (Figure 3), and then resolve the failure planes of the Wenchuan earthquake (Figure 4; Table S1). We explored an updated “cut and paste” (CAP) method (Zhu and Helmberger, 1996) on broadband waveform data of the regional Sichuan Digital Seismic Network (Yi et al., 2012). The source mechanism is obtained by applying a direct grid search through all possible solutions to find the global minimum of misfit between the observations and synthetics, allowing time shifts between portions of seismograms and synthetics. One of the advantages of this CAP technique is that it proves insensitive to velocity models and lateral crustal variation, we refer readers to Zhu and Helmberger (1996) for a more detailed description of the method. Comparison of the available depth distribution of the aftershocks shows a maximum scatter of ~2 km (Yi et al., 2012; Zheng et al., 2009).

It was previously suggested that the type of the focal mechanism solution shows characteristic of spatial segmentation for the aftershocks (Wang et al., 2009; Yi et al., 2012; Zheng et al., 2009). Three primary segments were primarily proposed along the main rupture zone from southwest to northeast, where initially the focal mechanism is of main thrust type, finally of main right-lateral strike-slip type and between these two areas there is a transition zone characterized in multiple types of focal mechanisms (Wang et al., 2009; Yi et al., 2012; see Figure 1 for segmentation boundaries). Analysis of failure planes derived from focal mechanisms of the aftershocks (Ms>4.0) therefore allows us to evaluate the orientation of nodal planes with depth for different segments (Figures 4) (Yi et al., 2012). The focal mechanisms of the aftershocks suggest, first, the fault planes for all segments have dips more than 40°, mostly up to 50–65° (Figure 4), and second, the aftershock sequence is segmented along the trace of the rupture. Along the southern segment, the dip of aftershock nodal planes appears to shallow progressively with increasing depth (60 – 70° between 3 – 13 km, and ~40° at ~18 km deep) (Figure 4a), consistent with the suggestion of a listric structure derived from geodetic observations (Shen et al., 2009). Along the central fault segment, the average dip appears to range from ~50 – 60° in the shallow crust to ~40° between 10 – 20 km depth (Figure 3b). But in the north, the sequence is consistent with a planar fault (50 – 65°) (Figures 4c). For the Beichuan fault, averaged angles of all the failure planes show a very steep, ~50-65°, fault geometry (Figures 4d), inconsistent with the reflection seismic observations.

In addition, two other lines of evidence lead us to argue that it is unlikely that the shallowly dipping faults observed in reflection seismic data were the primary fault responsible for the 2008 Wenchuan rupture. First, the positions of precisely located aftershocks define a cluster of seismicity concentrated between 12 – 20 km depth, but located directly below the surface trace of the rupture (Figure 2). If the rupture passed through the volume of rock exhibiting the aftershocks, they implicate a high-angle (~60°) fault (Figure 2a), which is consistent with our failure plane estimates (Figure 3a). Such a structure is not obvious in previous reflection seismic data (Jia et al., 2010; Y Li et al., 2010). We suspect it may be relatively transparent due to a combination of sparse data sampling and a high angle of the fault, which generates only weak reflections. Although seismic images are more complete across the northern portion of the rupture zone (Figure 2b) (Jia et al., 2010), there is still a large discrepancy between the position of the aftershock cluster and the position of the shallowly west-dipping Beichuan fault. Here, the aftershocks sit 8-10 km below the ~15 – 25° dipping Beichuan fault (present at ~7 km depth in Figure 2b). Given the ~2 km uncertainties of the aftershock locations (Yi et al., 2012; Zheng et al., 2009), all of the aftershocks are still ~6 – 8 km below the mapped Beichuan fault (Figure 2b). It seems clear that, although the surface trace of 2008 rupture is nearly coincident with the low-angle Beichuan fault, these are not the same structures at depth. Instead, our failure plane solution of a planar fault (50 – 65°) matches the aftershocks below the surface trace (Figures 2b, 4b and 4c). However, as shown in Figure 2, the distribution of earthquakes beneath the Longmen Shan forms a broad cloud. Given a maximum scatter of ~2 km of the aftershocks relocation for available different velocity models (Yi et al., 2012), we interpret this broad distribution of earthquakes to reflect a wide damage zone associated with deformation in the wall rocks.

Second, the detailed trace of the coseismic rupture along the Beichuan fault obliquely transects previously mapped faults near the northeastern tip (transparent thick blue dash-line in Figure 1), suggesting a crosscutting relationship between the steep rupture plane (Zhang et al., 2010) and the low-angle overthrusts in this region (Hubbard and Shaw, 2009; Hubbard et al., 2010; Jia et al., 2006, 2010). Near the northeastern terminus of the aftershocks, one branch of the two aftershock zones deviated northward from the Pingwu-Qingchuan fault (Figure 1), testifying to a newly-born feature of steeper fault cross-cutting the previously indentified faults. Interestingly, for the 2013 Lushan earthquake, available relocated aftershocks also appear to show a cross-cutting relationship between the surface fault trace and depth distribution of the aftershock sequence, similar to what we observed for the Wenchuan aftershocks across the Beichuan and Pingwu-Qingchuan faults (Figure 1).

In summary, guided by the pattern of the orientation of nodal planes with depth, we reexamined the aftershock depth distribution relative to structural interpretations of fault geometry based on seismic reflection data (Figures 2a and 2b) (Jia et al., 2006, 2010; Y Li et al., 2010). Our new interpretations suggest that the 2008 Wenchuan earthquake occurred along a structure that transects the upper 20 km of the crust at a relatively high angle (Figure 2). The inferred geometry requires that this fault system cross-cuts many, if not all, of the primary imbricate structures that comprise the fold-and-thrust belt along the Longmen Shan (Jia et al., 2006, 2010; Y Li et al., 2010) (Figure 2).

4. Discussion

Our analysis suggests that, although low-angle thrust faults are clearly imaged on seismic data (Hubbard and Shaw, 2009; Hubbard et al., 2010; Jia et al., 2010; Y Li et al., 2010), recently active faults appear to cross-cut these structures (Zhang et al., 2010; Zhu and Zhang, 2010, 2013) (Figures 2 and 4). Acquisition of high-resolution seismic profiles appears to confirm that the Beichuan fault (not Pengguan fault) along the central-northern Longmen Shan remains relatively high angle (>45 °) throughout the upper 5-6 km of the crust (Figure 1, Wu et al. 2014) and cross-cuts the previously imaged imbricate thrusts (Jia et al., 2006, 2010; Y Li et al., 2010). Along the southern Longmen Shan, a steep geometry of the Pengguan fault was proposed (Figure 5; Y Zhang et al., 2013), thus, we suggest that this may be characteristic of many of the active faults along the Longmen Shan mountain front. The clear difference in the pattern of aftershocks in the north vs. the south suggests that a new, vertical strike-slip fault ruptured in the north, while the southern part of the rupture occurred on a slightly gently dipping (~50 – 65 degrees) plane, which indicates an along-strike variation of the fault geometry (Figure 4), as also evidenced by the contrasting landscapes along the Longmen Shan (Kirby et al., 2003; Zhang et al., 2011). It is also clear that the Beichuan fault has accumulated displacement prior the 2008 Wenchuan earthquake; both deformed fluvial terraces and trenches (Ran et al., 2010, 2013) indicate sustained fault during the late Quaternary. Moreover, differences in the cooling history of the hanging wall block (e.g. Wang et al., 2012) and footwall block (e.g., Arne et al., 1997) suggest that fault activity may extend back to the late Miocene. Thus, we hypothesize that the presently active high-angle faults have accumulated displacement for a significant length of geologic time.

Further, our hypothesis that seismogenic faults in the Longmen Shan are newly formed, high-angle structures has important implications for seismic hazards along this mountain front. First, the geometry of the fault influences the rate of strain accumulation during interseismic deformation. Shortening across the Longmen Shan, prior to the 2008 Wenchuan earthquake, was inferred from geodetic studies to be low, on the order of 1-3 mm/yr (Gan et al., 2007; Zhang et al., 2010). Trenching and associated dating along the Beichuan fault revealed ~3,000 years of recurrence similar to the Wenchuan earthquake, therefore, the ~5 m observed average coseismic displacement during the 2008 event requires an average rate of ~1.7 mm/yr deformation (Ran et al., 2010, 2013). More specifically, at Yingxiu trench site, and ~7.6 m cumulative vertical displacement (including ~2.4 m coseismic offset) during the last ~6,000 year confirms an average dip-slip rate of ~0.9 mm/yr (Ran et al., 2010, 2013). Although the Holocene slip rate along the Beichuan fault is not well determined, it appears to be on the order of ~1 mm/yr (Densmore et al., 2007). All of these estimates of vertical motion along the fault system are similar to rates of erosion (>0.3 – 0.4 mm/yr) in the hanging wall block (Kirby and Ouimet, 2011). The close correspondence between erosion rates in the hanging wall and the throw rate along the Beichuan fault also argues for a relatively long-lived, high-angle structure.

Second, although the Cenozoic evolution of shortening across the Longmen Shan foreland has been suggested to reflect a forward-propagating sequence of deformation within the Sichuan Basin (Figure 1) (Chen et al., 2013; Cook et al., 2013; Hubbard and Shaw, 2009; Tan et al., 2014; Wang et al., 2013), both the Wenchuan and Lushan earthquakes occurred in an "out-of-sequence" position in the hinterland of the range. The absence of a surface rupture during the 2013 Lushan event (Xu et al., 2013; Z Zhang et al., 2013) has led to an active debate still ongoing over whether slip occurred on the Pengguan fault or on one of the faults father east in the foreland (Wang et al., 2014; Xu et al., 2013; Y Zhang et al., 2013). The close correspondence of the epicentral locations with the Pengguan fault (Shuangshi-Dachuan fault) suggest that this event was also possibly hosted along a relatively steep structure (Figures 1 and 5; Y Zhang et al., 2013). Indeed, available trenches along the fault revealed that the

Shuangshi-Dachuan fault has been active in the Holocene, and there were one or more larger surface-breaking events during the past millennial period (Chen et al., 2013; Densmore et al., 2007). Those early events, although maybe slightly bigger than the Lushan earthquake, were mostly resulted from the slip along the high-angle Pengguan fault, identical to the latest 2013 event (Figure 5; Y Zhang et al., 2013).

Some of the low-angle structures within the Sichuan Basin are indeed active. A number of small earthquakes have occurred along the trace of the Longquan anticline (Burchfiel et al., 2008), and deformation of Quaternary deposits in the Dayi region (Li et al., 2014; Wang et al., 2014) suggest relatively slow shortening along faults within the basin. It appears that many of these structures root into a subhorizontal décollement at < 10 km (Z Li et al., 2013; Wang et al., 2014), and it appears that this structure f at the Longmen Shan range front remains active during shortening along high-angle faults further into the interior Longmen Shan range.

Despite this, our results highlight that potential exists for additional rupture along these high-angle faults, such as the Wenchuan-Maoxian fault and along the ~60 km seismic gap between Wenchuan and Lushan earthquakes (Figure 1) (Chen et al., 2013; Li et al., 2014; Xu et al., 2013). Our analysis of recent seismic events, including the July 22nd, 2013 Minxian-Zhangxian *M*w 6.0 earthquake (Zheng et al., 2013), suggests that significant seismic hazard along eastern margin of the plateau arises from deep-seated, steeply dipping faults.

We suggest that many (but not all) of the low-angle thrust faults imaged on seismic data may not be the primary active structures, and that the next generation of seismic hazard evaluations needs consider the role of high-angle reverse faults in the overall deformation field.

5. Conclusion

We obtained failure planes for the 2008 Wenchuan earthquake by analyzing the focal mechanisms of low-magnitude aftershock events. For all segments along the Beichuan fault, we observe that the coseismic fault dips greater than 40°, and primarily 50 – 65°. Reinterpreting the aftershock sequence along the trace of the rupture, along with our synthesis of the aftershock distribution and subsurface fault geometries, lead us to conclude that present-day fault activity and aftershocks are concentrated along relatively high-angle structures. These faults appear to cross-cut primary low-angle faults imaged in reflection seismic data along the Longmen Shan and in the Sichuan Basin. We suggest that the crustal scale low-angle thrust faulting model and the high-angle listric reverse fault are both correct, but that low-angle thrusts are largely antecedent and may not represent the primary seismic hazard in the region. Seismogenic deformation along the Longmen Shan is accomplished along high-angle, listric structures. Thus, our current models of faults responsible for the earthquakes along the heavily populated Sichuan Basin need to be further explored to represent the distribution of subsurface seismic hazard.

Acknowledgements. We gratefully acknowledge Clark Burchfiel and two anonymous reviewers for constructive reviews and suggestions. This research was supported by the Sichuan Seistech Corporation Ltd. (XDK2015001), Ministry of National Science and Technology (Grant no. 2012BAK19B01-01) and National Science Foundation of China (Grant no. 41272196, 41030317). We further benefit discussions with Xueze Wen, Jing Liu, Zhuqi Zhang and Honglin He.

References

Arne, D., Worley, B., Wilson, C., Chen, S., Foster, D., Luo, Z., Liu, S., Dirks, P., 1997. Differential exhumation in response to episodic thrusting along the eastern margin of the Tibetan Plateau. Tectonophysics 280, 239-256.

Bai, D., Unsworth, M.J., Meju, M.A., Ma, X., Teng, J., Kong, X., Sun, Y., Sun, J., Wang, L., Jiang, C., Zhao, C., Xiao, P., Liu, M., 2010. Crustal deformation of the eastern Tibetan plateau revealed by magnetotelluric imaging. Nature Geoscience 3, 358-362.

Bilham, R. 2004. Earthquakes in India and the Himalaya: tectonics, geodesy and history. Annals of Geophysics 47(2), 839-858.

Burchfiel, B.C., Chen, Z., Liu, Y., Royden, L.H., 1995. Tectonics of the Longmen Shan and Adjacent Regions, Central China. International Geology Review 37, 661-735.

Burchfiel, B.C., Royden, L.H., van der Hilst, R.D., Hager, B.H., Chen, Z., King, R.W., Li, C., Lu, J., Yao, H.J., Kirby, E., 2008. A geological and geophysical context for the Wenchuan earthquake of 12 May 2008, Sichuan, People' s Republic of China. GSA Today 18, 4-11.

Chen, L., Ran, Y., Wang, H., Li, Y., Ma, X., 2013. The Lushan Ms 7.0 earthquake and activity of the southern segment of the Longmenshan fault zone. Chinese Science Bulletin 58, 1925-1932.

Chen, S., Wilson, C.J.L., 1996. Emplacement of the Longmen Shan Thrust-Nappe Belt along the eastern margin of the Tibetan Plateau. Journal of Structural Geology 18, 413-430.

Chen, S., Wilson, C.J.L., Worley, B.A., 1995. Tectonic transition from the Songpan-Garzê Fold Belt to the Sichuan Basin, south-western China. Basin Research 7, 235-253.

Chen, Z., Burchfiel, B.C., Liu, Y., King, R.W., Royden, L.H., Tang, W., Wang, E., Zhao, J., Zhang, X., 2000. Global Positioning System measurements from eastern Tibet and their implications for India/Eurasia intercontinental deformation. J Geophys Res-Sol Ea 105, 16215-16227.

Clark, M.K., House, M.A., Royden, L.H., Whipple, K.X., Burchfiel, B.C., Zhang, X., Tang, W., 2005. Late Cenozoic uplift of southeastern Tibet. Geology 33, 525-528.

Clark, M.K., Royden, L.H., 2000. Topographic ooze: Building the eastern margin of Tibet by lower crustal flow. Geology 28, 703-706.

Cook, K.L., Royden, L.H., Burchfiel, B.C., Lee, Y.-H., Tan, X., 2013.

Constraints on Cenozoic tectonics in the southwestern Longmen Shan from low-temperature thermochronology. Lithosphere 5, 393-406.

Deng, Q. D, 2007. Ed. Map of the Active faults in China: 1:4,000,000. Seismological Press.

Densmore, A.L., Ellis, M.A., Li, Y., Zhou, R.J., Hancock, G.S., Richardson, N., 2007. Active tectonics of the Beichuan and Pengguan faults at the eastern margin of the Tibetan Plateau. Tectonics 26,(4), Doi 10.1029/2006tc001987.

Dirks, P.H.G.M., Wilson, C.J.L., Chen, S., Luo, Z.L., Liu, S., 1994. Tectonic evolution of the NE margin of the Tibetan Plateau; evidence from the central Longmen Mountains, Sichuan Province, China. Journal of Southeast Asian Earth Sciences 9, 181-192.

Fang, L., Wu, J., Wang, W., Lu, Z., Wang, C., Yang, T., Cai, Y., 2013. Relocation of mainshock and aftershock sequences of Ms7.0 Sichuan Lushan earthquake. Chinese Science Bulletin 58, 1901-1909.

Feng, G., Hetland, E.A., Ding, X., Li, Z., Zhang, L., 2010. Coseismic fault slip of the 2008 Mw 7.9 Wenchuan earthquake estimated from InSAR and GPS measurements. Geophysical Research Letters 37, L01302.

Fu, B., Shi, P., Guo, H., Okuyama, S., Ninomiya, Y., Wright, S., 2011. Surface deformation related to the 2008 Wenchuan earthquake, and mountain building of the Longmen Shan, eastern Tibetan Plateau. Journal of Asian Earth Sciences 40, 805-824.

Gan, W., Zhang, P., Shen, Z., Niu, Z., Wang, M., Wan, Y., Zhou, D., Cheng, J.,

2007. Present-day crustal motion within the Tibetan Plateau inferred from GPS measurements. J Geophys Res-Sol Ea 112, B08416.

Hao, K.X., Si, H.J., Fujiwara, H., Ozawa, T., 2009. Coseismic surface-ruptures and crustal deformations of the 2008 Wenchuan earthquake Mw7.9, China. Geophysical Research Letters 36.

Hubbard, J., Shaw, J.H., 2009. Uplift of the Longmen Shan and Tibetan plateau, and the 2008 Wenchuan (M=7.9) earthquake. Nature 458, 194-197.

Hubbard, J., Shaw, J.H., Klinger, Y., 2010. Structural Setting of the 2008 Mw 7.9 Wenchuan, China, Earthquake. Bulletin of the Seismological Society of America 100, 2713-2735.

Jia, D., Li, Y., Lin, A., Wang, M., Chen, W., Wu, X., Ren, Z., Zhao, Y., Luo, L., 2010. Structural model of 2008 M-w 7.9 Wenchuan earthquake in the rejuvenated Longmen Shan thrust belt, China. Tectonophysics 491, 174-184.

Jia, D., Wei, G., Chen, Z., Li, B., Zeng, Q., Yang, G., 2006. Longmen Shan fold-thrust belt and its relation to the western Sichuan Basin in central China: New insights from hydrocarbon exploration. AAPG Bulletin 90, 1425-1447.

Kirby, E., Ouimet, W., 2011. Tectonic geomorphology along the eastern margin of Tibet: insights into the pattern and processes of active deformation adjacent to the Sichuan Basin, in: Gloaguen, R.R.L. (Ed.), Growth and Collapse of the Tibetan Plateau, pp. 165-188.

Kirby, E., Reiners, P.W., Krol, M.A., Whipple, K.X., Hodges, K.V., Farley, K.A., Tang, W., Chen, Z., 2002. Late Cenozoic evolution of the eastern margin of the Tibetan Plateau: Inferences from 40Ar/ 39Ar and (U-Th)/He thermochronology. Tectonics 21.

Kirby, E., Whipple, K.X., Tang, W., Chen, Z., 2003. Distribution of active rock uplift along the eastern margin of the Tibetan Plateau: Inferences from bedrock channel longitudinal profiles. J Geophys Res-Sol Ea 108.

Li, C., Wei, Z., Ye, J., Han, Y., Zheng, W., 2010. Amounts and styles of coseismic deformation along the northern segment of surface rupture, of the 2008 Wenchuan Mw 7.9 earthquake, China. Tectonophysics 491, 35-58.

Li, H., Wang, H., Xu, Z., Si, J., Pei, J., Li, T., Huang, Y., Song, S.-R., Kuo, L.-W., Sun, Z., Chevalier, M.-L., Liu, D., 2013. Characteristics of the fault-related rocks, fault zones and the principal slip zone in the Wenchuan Earthquake Fault Scientific Drilling Project Hole-1 (WFSD-1). Tectonophysics 584, 23-42.

Li, Y., Jia, D., Shaw, J.H., Hubbard, J., Lin, A., Wang, M., Luo, L., Li, H., Wu, L., 2010. Structural interpretation of the coseismic faults of the Wenchuan earthquake: Three-dimensional modeling of the Longmen Shan fold-and-thrust belt. Journal of Geophysical Research: Solid Earth 115, B04317.

Li, Y., Jia, D., Wang, M., Shaw, J.H., He, J., Lin, A., Xiong, L., Rao, G., 2014. Structural geometry of the source region for the 2013 Mw 6.6 Lushan earthquake: Implication for earthquake hazard assessment along the Longmen Shan. Earth Planet Sc Lett 390, 275-286.

Li, Z., Jia, D., Chen, W., 2013. Structural geometry and deformation mechanism of the Longquan anticline in the Longmen Shan fold-and-thrust belt, eastern Tibet. Journal of Asian Earth Sciences 64, 223-234.

Liu-Zeng, J., Zhang, Z., Wen, L., Tapponnier, P., Sun, J., Xing, X., Hu, G., Xu, Q., Zeng, L., Ding, L., Ji, C., Hudnut, K.W., van der Woerd, J., 2009. Co-seismic ruptures of the 12 May 2008, Ms 8.0 Wenchuan earthquake, Sichuan: East–west crustal shortening on oblique, parallel thrusts along the eastern edge of Tibet. Earth Planet Sc Lett 286, 355-370.

Loveless, J.P., Meade, B.J., 2011. Partitioning of localized and diffuse deformation in the Tibetan Plateau from joint inversions of geologic and geodetic observations. Earth Planet Sc Lett 303, 11-24.

McClay, K.R, 1989. Analogue models of inversion tectonics. In: Cooper Ma and Williams G. D. (Eds), Inversion Tectonics. Geol Soc London Spec Pub, *44*, 41-59.

Ran, Y., Chen, L., Chen, J., Wang, H., Chen, G., Yin, J., Shi, X., Li, C., Xu, X., 2010. Paleoseismic evidence and repeat time of large earthquakes at three sites along the Longmenshan fault zone. Tectonophysics 491, 141-153.

Ran, Y., Chen, W., Xu, X., Chen, L., Wang, H., Yang, C., Dong, S., 2013. Paleoseismic events and recurrence interval along the Beichuan–Yingxiu fault of Longmenshan fault zone, Yingxiu, Sichuan, China. Tectonophysics 584, 81-90.

Richardson, N.J., Densmore, A.L., Seward, D., Fowler, A., Wipf, M., Ellis, M.A., Yong, L., Zhang, Y., 2008. Extraordinary denudation in the Sichuan Basin: Insights from low-temperature thermochronology adjacent to the eastern margin of the Tibetan Plateau. Journal of Geophysical Research: Solid Earth 113, B04409.

Robert, A., Pubellier, M., de Sigoyer, J., Vergne, J., Lahfid, A., Cattin, R., Findling, N., Zhu, J., 2010b. Structural and thermal characters of the Longmen Shan (Sichuan, China). Tectonophysics 491, 165-173.

Robert, A., Zhu, J., Vergne, J., Cattin, R., Chan, L.S., Wittlinger, G., Herquel, G., de Sigoyer, J., Pubellier, M., Zhu, L.D., 2010a. Crustal structures in the area of the 2008 Sichuan earthquake from seismologic and gravimetric data. Tectonophysics 491, 205-210.

Royden, L.H., Burchfiel, B.C., King, R.W., Wang, E., Chen, Z., Shen, F., Liu, Y., 1997. Surface deformation and lower crustal flow in eastern Tibet. Science 276, 788-790.

Shen, Z., Sun, J., Zhang, P., Wan, Y., Wang, M., Burgmann, R., Zeng, Y., Gan, W., Liao, H., Wang, Q., 2009. Slip maxima at fault junctions and rupturing of barriers during the 2008 Wenchuan earthquake. Nature Geoscience 2, 718-724.

Tan, X., Lee, Y.-H., Chen, W., Cook, K.L., Xu, X., 2014. Exhumation history and faulting activity of the southern segment of the Longmen Shan, eastern Tibet. Journal of Asian Earth Sciences 81, 91-104.

Wang, E., Kirby, E., Furlong, K.P., van Soest, M., Xu, G., Shi, X., Kamp, P.J.J., Hodges, K.V., 2012. Two-phase growth of high topography in eastern Tibet during the Cenozoic. Nature Geosci 5, 640-645.

Wang, M., Jia, D., Shaw, J.H., Hubbard, J., Lin, A., Li, Y., Shen, L., 2013. Active Fault□Related Folding beneath an Alluvial Terrace in the Southern Longmen Shan Range Front, Sichuan Basin, China: Implications for Seismic Hazard. Bulletin of the Seismological Society of America 103, 2369-2385.

Wang, M., Jia, D., Shaw, J.H., Hubbard, J., Plesch, A., Li, Y., Liu, B., 2014. The 2013 Lushan earthquake: Implications for seismic hazards posed by the Range Front blind thrust in the Sichuan Basin, China. Geology 42, 915-918.

Wang, Q., Chen, Z., Zheng, S., 2009. Spatial segmentation characteristic of focal mechanism of aftershock sequence of Wenchuan Earthquake. Chinese Science Bulletin 54 (16), 2263-2270.

Wang, W., Zhao, L., Li, J., Yao, Z., 2008. Rupture process of the Ms 8.0 Wenchuan earthquake of Sichuan, China. Chinese Journal of Geophysics-Chinese Edition 51, 1403-1410.

Wobus, C., Whipple, K.X., Kirby, E., Snyder, N., Johnson, J., Spyropolou, K., Crosby, B., Sheehan, D., 2006. Tectonics from topography: Procedures, promise, and pitfalls. Geological Society of America Special Papers 398, 55-74.

Wu, C., Li, H., Leloup, P.H., Yu, C., Si, J., Liu, D., Pan, J., Chevalier, M.-L., Gong, Z., 2014. High-angle fault responsible for the surface ruptures along the northern segment of the Wenchuan Earthquake Fault Zone: Evidence from the latest seismic reflection profiles. Tectonophysics 619–620, 159-170.

Xu, X., Wen, X., Han, Z., Chen, G., Li, C., Zheng, W., Zhang, S., Ren, Z., Xu, C., Tan, X., Wei, Z., Wang, M., Ren, J., He, Z., Liang, M., 2013. Lushan Ms 7.0 earthquake: A blind reserve-fault event. Chinese Science Bulletin 58, 1887-1893.

Xu, X., Wen, X., Yu, G., Chen, G., Klinger, Y., Hubbard, J., Shaw, J., 2009. Coseismic reverse- and oblique-slip surface faulting generated by the 2008 Mw 7.9 Wenchuan earthquake, China. Geology 37, 515-518.

Yi, G., Long, F., Zhang, Z., 2012. Spatial and temporal variation of focal mechanisms for aftershocks of the 2008 M(s)8. 0 Wenchuan earthquake. Chinese Journal of Geophysics-Chinese Edition 55, 1213-1227.

Zhang, H., Zhang, P., Kirby, E., Yin, J., Liu, C., Yu, G., 2011. Along-strike topographic variation of the Longmen Shan and its significance for landscape evolution along the eastern Tibetan Plateau. Journal of Asian Earth Sciences 40, 855-864.

Zhang, P., 2013. Beware of slowly slipping faults. Nature Geosci 6, 323-324.

Zhang, P., Shen, Z., Wang, M., Gan, W., Burgmann, R., Molnar, P., 2004. Continuous deformation of the Tibetan Plateau from global positioning system data. Geology 32, 809-812.

Zhang, P., Wen, X., Shen, Z., Chen, J., 2010. Oblique, High-Angle, Listric-Reverse Faulting and Associated Development of Strain: The Wenchnan Earthquake of May 12, 2008, Sichuan, China. Annual Review of

Earth and Planetary Sciences 38, 353-382.

Zhang, Y., Dong, S., Hou, C., Shi, J., Wu, Z., Li, H., Sun, P., Liu, G., Li, J., 2013. Seismogenic structure of the April 20, 2013, Lushan Ms7 earthquake in Sichuan. Acta Geologica Sinica (English Edition) 87, 633-645.

Zhang, Z., Wang, W., Ren, Z., Zhang, P., Fang, L., Wu, J., 2013. Lushan MS7.0 earthquake: A special earthquake occurs on curved fault. Chinese Science Bulletin 58, 3483-3490.

Zhao, G., Unsworth, M.J., Zhan, Y., Wang, L., Chen, X., Jones, A.G., Tang, J., Xiao, Q., Wang, J., Cai, J., Li, T., Wang, Y., Zhang, J., 2012. Crustal structure and rheology of the Longmenshan and Wenchuan Mw 7.9 earthquake epicentral area from magnetotelluric data. Geology 40, 1139-1142.

Zheng, W., Yuan, D., He, W., Min, W., Ren, Z., Liu, X., Wang, A., Xu, C., Ge, W., Li, F., 2013. Geometric pattern and active tectonics in Southeastern Gansu province：Discussion on seismogenic mechanism of the Minxian-Zhangxian Ms6.6 earthquake on July 22,2013. Chinese Journal Geophysics 56, 4058-4071.

Zheng, Y., Ma, H., Lü, J., Ni, S., Li, Y., Wei, S., 2009. Source mechanism of strong aftershocks (M s>=5.6) of the 2008/05/12 Wenchuan earthquake and the implication for seismotectonics. Science in China Series D: Earth Sciences 52, 739-753.

Zhu, L., Helmberger, D.V., 1996. Advancement in source estimation techniques using broadband regional seismograms. Bulletin of the Seismological Society of America 86, 1634-1641.

Zhu, S., Zhang, P., 2010. Numeric Modeling of the Strain Accumulation and Release of the 2008 Wenchuan, Sichuan, China, Earthquake. Bulletin of the Seismological Society of America 100, 2825-2839.

Zhu, S., Zhang, P., 2013. FEM simulation of interseismic and coseismic deformation associated with the 2008 Wenchuan Earthquake. Tectonophysics 584, 64-80.

Figure captions

Figure 1

Distribution of the seismogenic Longmen Shan faults in eastern Tibet. Black lines are previously identified faults (Xu et al., 2009; Zhang et al., 2010). Red lines represent two coseismic ruptures along the Beichuan and Penguan faults (Xu et al., 2009; Zhang et al., 2010) during the 2008 *M*w 7.9 Wenchuan earthquake. Color-coded circles are series of the Wenchuan aftershocks (red and blue) and Lushan aftershocks (yellow-brown) until April, 2013. Southern, central and northern segments of the Longmen Shan faults are separated by white lines and aftershocks in red were selected to infer the failure planes for associated segements (Yi et al., 2012). Three purple lines marked by AA', BB' and CC' are locations of the seismic reflection profiles by Jia et al. (2010) and

Wang et al. (2014). Three shorter yellow lines are much higher resolution reflection profiles by Wu et al., 2014. Inset map shows the tectonic location of the Longmen Shan relative to the Tibetan Plateau (gray-shaded region). Cd, Chengdu; Ax, Anxian; Bc, Beichuan; Bx,Baoxing; Dj,Dujiangyan; Dy, Dayi; Jy, Jiangyou; Ls, Lushan; Lx, Lixian; Mx, Maoxian; Pw, Pingwu; Qc, Qingchuan; Sp, Songpan; Wc, Wenchuan; Ya, Yaan

Figure 2

Explanation of the coseismic Beichuan and Pengguan faults (red lines) by seismic reflection data, typically characterized by low-angle imbricated overthrust geometry (Jia et al., 2006, 2010; Y Li et al., 2010), and our new interpretations of the high-angle fault geometry (black dashed lines) according to reflection data and the dip/depth relations for southern and northern Longmen Shan faults (Wu et al., 2014, Yi et al., 2012).

Figures 3

Example of waveform fitting and focal mechanism determination (2011 May 6 *M*w4.1 aftershock)

(a) Comparison of synthetic waveforms with observations. Red and black lines are synthetics and observations, respectively. Numbers are time shifts of the synthetics relative to the observations and the corresponding cross-correlation coefficients (in percentage); (b) Fitting error as a function of focal depth. Note the best focal mechanism at 8 km depth with a minimum error.

Figure 4

Failure planes for different fault segments (a-c) and the Beichuan fault (d) derived from focal mechanisms of the aftershocks (Yi et al., 2012), S, C, N and A represents southern (a), central (b), northern (c) segments and all the fault (d). Red dots are averaged dip angles for two failure planes within 1-km depth, and gray triangles above error bars are the mean dip angles for each minimum and maximum values. Aftershocks are *M*s larger than 4.0 and prior to April, 2014, red color-coded in Figure 1. Note that the fault planes for all segments have dips more than 40°, mostly up to 50–65°, in contrast with the fault geometry imaged by seismic reflection in Figure 2.

Figure 5

Reinterpretation of the high-angle coseismic Shuangshi-Dachuan (Pengguan) fault (black dashed line) (Y Zhang et al., 2013), crosscutting low-angle imbricated overthrust faults revealed by seismic reflection data (Wang et al., 2014).

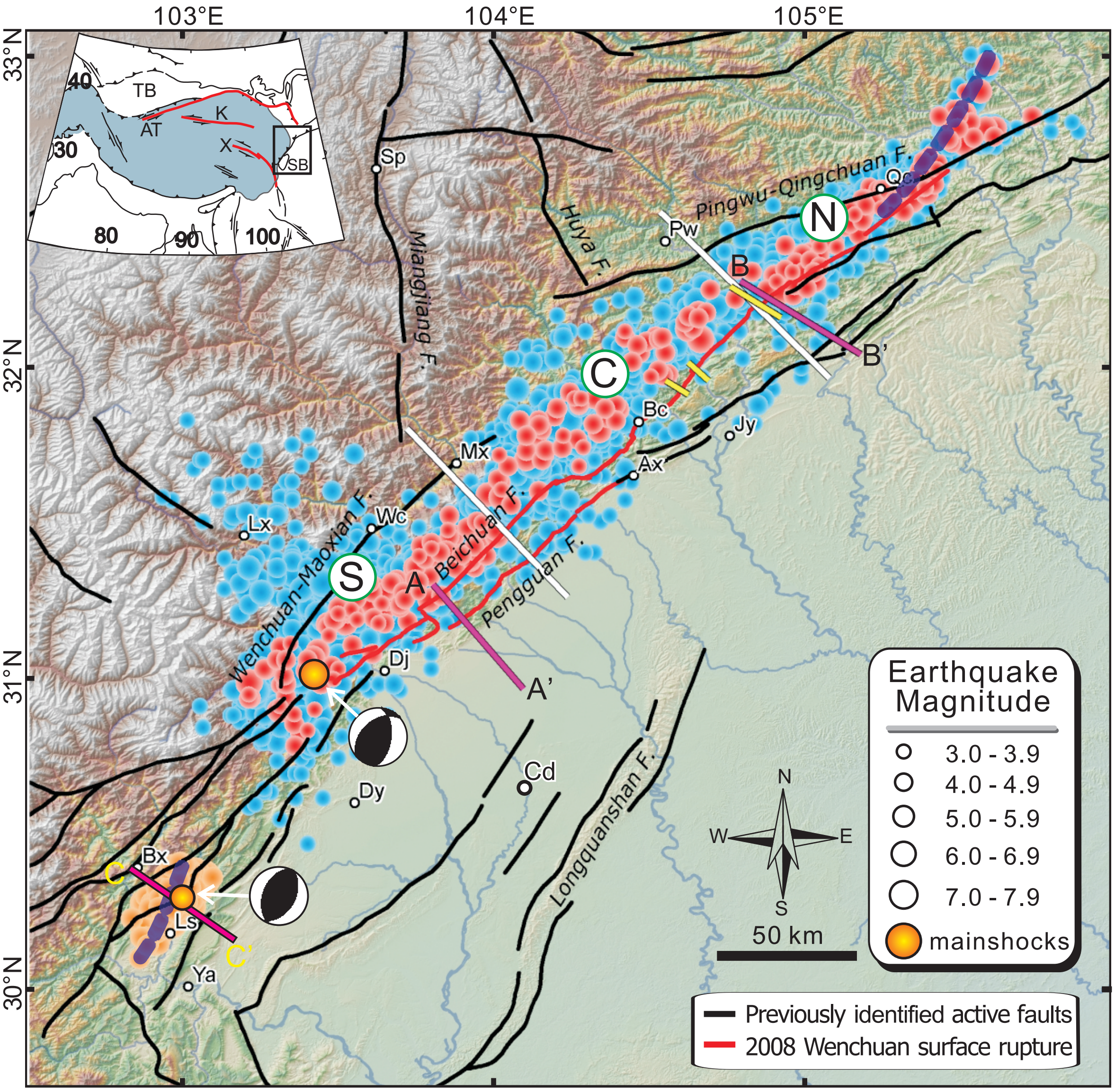

Zhang et al., Figure 1

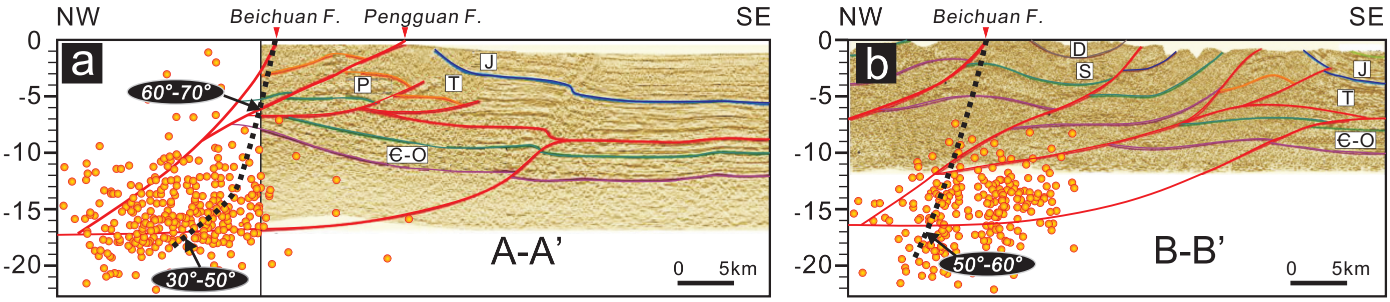

Zhang et al., Figure 2

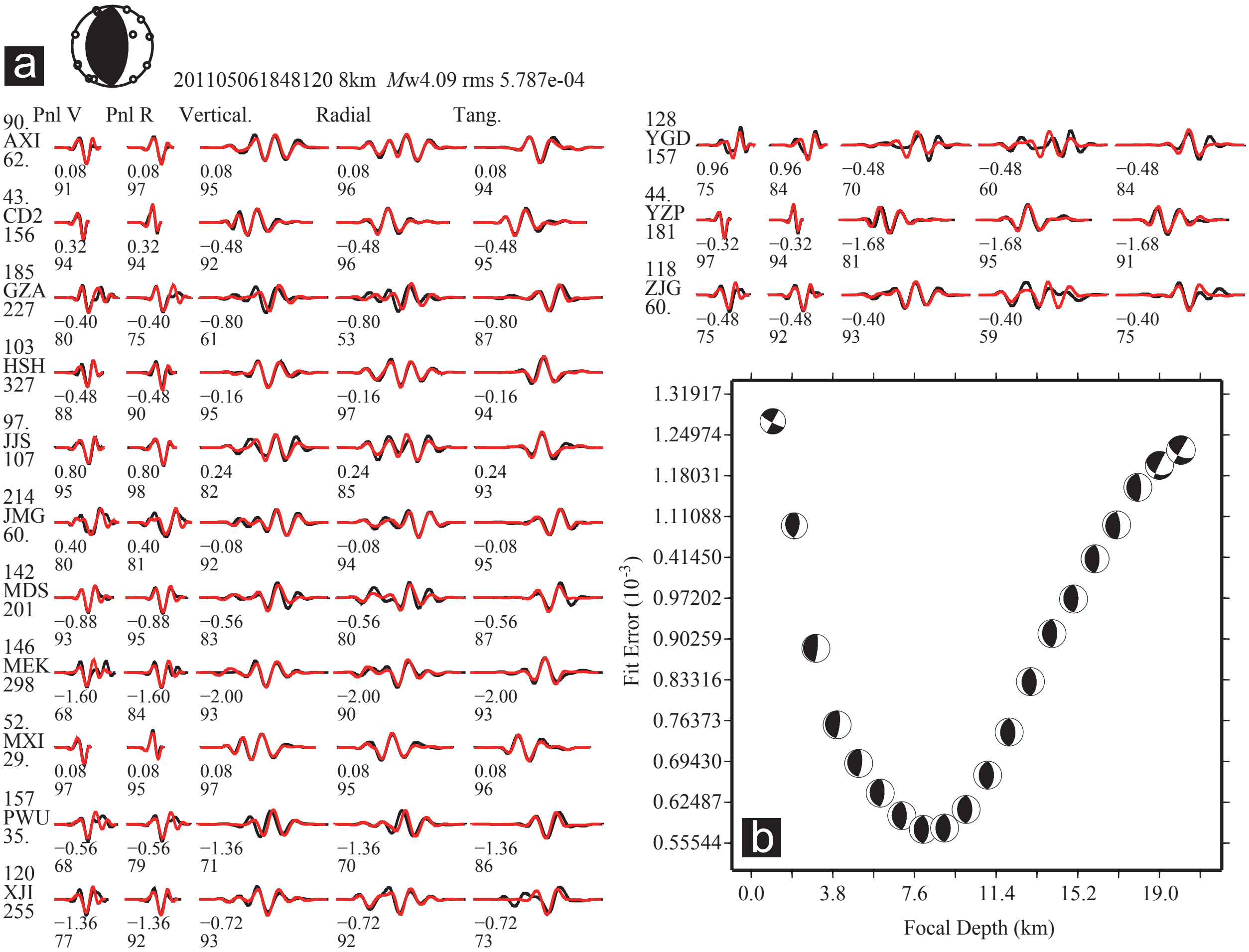

Zhang et al., Figure 3

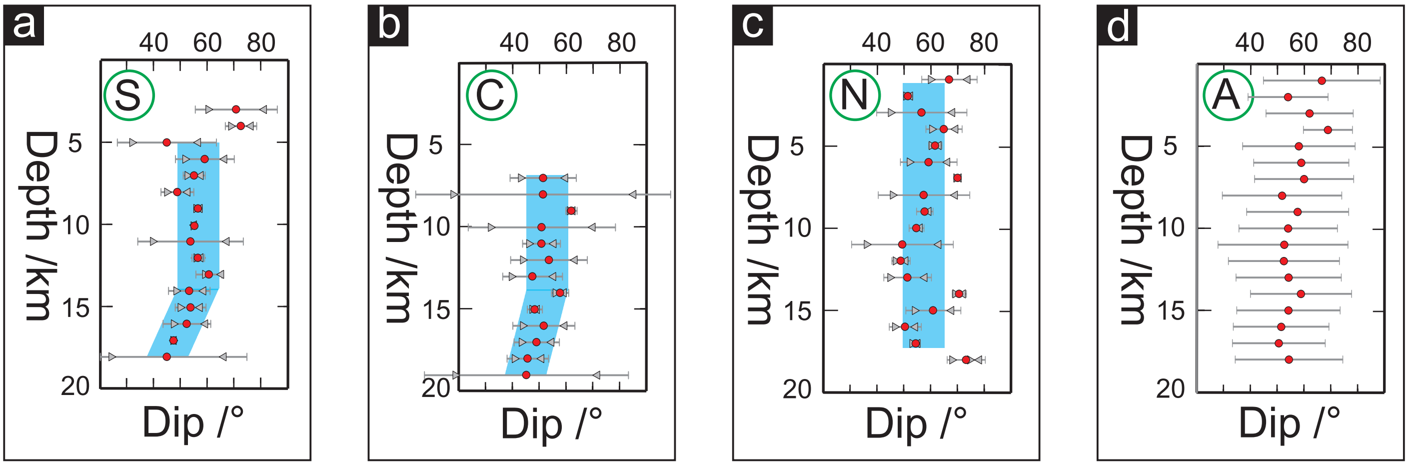

Zhang et al., Figure 4

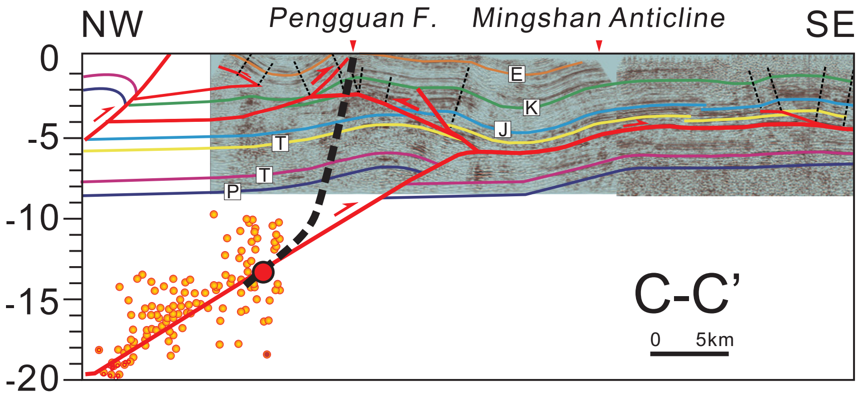

Zhang et al., Figure 5

Supplementary material

Table S1 Aftershocks (Ms>4.0) of the Wenchuan earthquake and dip angles of the failure planes for relevant aftershocks along the Beichuan fault.

Aftershock No.	Longitude /°	Latitude /°	Magnitude	Depth /km	Failure plane dip angles	
					Plane I /°	Plane II /°
1	105.58	32.99	5.5	1	71	35
2	104.89	32.28	4.0	1	84	77
3	105.50	32.83	5.6	2	62	35
4	105.48	32.82	4.5	2	67	41
5	104.81	32.31	4.5	2	64	42
6	105.42	32.82	4.5	2	59	54
7	105.55	32.90	5.1	2	64	39
8	104.76	32.32	4.2	2	75	65
9	105.47	32.80	6.1	2	66	25
10	105.24	32.58	4.2	3	75	35
11	105.27	32.53	4.5	3	67	49
12	103.89	31.48	4.3	3	90	49
13	104.77	32.32	4.0	3	63	50
14	103.61	31.25	4.6	3	73	71
15	103.30	31.05	4.1	4	66	56
16	105.49	32.83	6.0	4	72	56
17	103.47	31.20	4.0	4	81	59
18	105.42	32.67	4.0	4	61	59
19	105.25	32.55	5.4	4	71	61
20	105.16	32.52	4.5	4	76	62
21	103.61	31.23	4.0	4	81	65
22	103.62	31.27	4.2	4	80	68
23	103.49	31.21	4.2	4	87	82
24	105.17	32.48	4.2	5	79	26
25	105.41	32.65	4.0	5	54	37
26	103.69	31.18	4.8	5	58	32
27	104.95	32.34	4.6	5	69	66
28	105.18	32.55	4.7	5	90	71
29	105.39	32.69	4.3	6	72	24
30	103.77	31.41	4.0	6	70	30
31	103.62	31.17	4.4	6	68	31
32	103.77	31.25	5.0	6	47	43
33	104.86	32.26	4.4	6	47	45
34	105.33	32.58	4.3	6	74	50
35	105.52	32.80	4.5	6	62	51

36	103.91	31.42	4.1	6	75	67
37	105.17	32.55	4.1	6	87	69
38	105.37	32.59	4.0	6	71	57
39	103.45	31.03	4.6	6	86	74
40	103.28	30.97	4.9	7	60	30
41	103.41	30.97	4.2	7	63	31
42	105.46	32.73	4.7	7	56	34
43	104.25	31.68	4.0	7	62	39
44	103.30	30.97	4.3	7	46	45
45	104.26	31.74	4.0	7	58	46
46	105.15	32.50	4.0	7	67	47
47	103.47	31.22	4.1	7	87	50
48	103.80	31.26	4.3	7	55	35
49	103.19	30.93	4.8	7	61	32
50	103.67	31.23	4.5	7	65	56
51	105.50	32.83	4.9	7	87	71
52	103.24	31.02	4.9	7	85	81
53	105.48	32.78	4.4	7	86	67
54	105.21	32.54	4.2	7	86	70
55	105.41	32.66	4.1	7	90	77
56	105.35	32.64	4.7	8	82	13
57	103.58	31.27	4.1	8	56	34
58	103.18	30.98	6.1	8	49	41
59	105.38	32.57	5.0	8	50	41
60	103.30	30.93	4.6	8	51	41
61	103.29	31.00	4.2	8	50	46
62	103.36	31.01	4.3	8	64	57
63	104.54	31.98	4.3	8	80	14
64	105.47	32.84	4.7	8	82	76
65	104.30	31.90	4.5	8	90	21
66	103.28	30.88	5.0	9	67	24
67	103.18	30.92	4.3	9	57	34
68	103.52	31.20	4.3	9	58	35
69	104.95	32.27	4.3	9	51	39
70	104.95	32.24	4.5	9	51	40
71	105.37	32.67	4.1	9	71	40
72	103.33	30.87	4.0	9	47	43
73	105.30	32.51	4.3	9	47	45
74	104.90	32.25	6.0	9	49	41
75	104.68	32.26	4.5	9	53	50
76	103.48	31.23	4.3	9	83	51
77	105.09	32.39	4.0	9	74	53
78	105.35	32.62	4.0	9	55	39
79	104.37	31.83	4.3	9	55	45

80	104.99	32.26	4.2	9	59	31
81	103.74	31.42	4.5	9	65	34
82	105.11	32.46	4.5	9	87	67
83	103.33	30.77	4.3	9	75	56
84	105.03	32.37	4.5	9	78	75
85	105.37	32.65	4.6	9	80	10
86	105.10	32.50	4.0	9	82	71
87	103.67	31.22	4.5	9	82	76
88	104.66	32.18	4.2	9	85	83
89	103.46	31.18	5.1	9	90	41
90	105.17	32.49	4.8	9	90	73
91	104.64	32.09	6.1	10	79	16
92	103.57	31.30	4.1	10	79	24
93	103.18	30.94	4.0	10	62	28
94	104.20	31.74	4.1	10	59	31
95	105.01	32.31	4.2	10	55	35
96	104.64	32.16	4.1	10	63	36
97	103.91	31.35	4.6	10	52	38
98	103.34	30.82	4.7	10	50	40
99	103.37	30.82	4.0	10	50	40
100	103.44	31.16	4.3	10	51	40
101	105.00	32.35	4.4	10	80	41
102	104.25	31.88	4.8	10	80	42
103	105.45	32.74	4.3	10	53	38
104	103.55	31.25	4.7	10	54	36
105	105.48	32.81	4.8	10	59	46
106	104.88	32.30	4.8	10	60	30
107	105.03	32.33	4.4	10	60	42
108	105.02	32.28	4.5	10	60	60
109	103.95	31.39	4.3	10	68	40
110	103.63	31.24	4.6	10	70	27
111	103.77	31.32	4.5	10	70	43
112	103.37	31.05	4.1	10	86	75
113	103.73	31.27	4.0	10	79	60
114	103.45	30.99	4.0	10	86	82
115	105.12	32.47	4.5	10	84	70
116	103.69	31.25	4.1	11	88	3
117	103.46	31.18	4.6	11	80	19
118	103.94	31.48	4.9	11	70	20
119	103.33	30.84	4.3	11	76	20
120	104.38	31.86	4.9	11	80	20
121	104.30	31.82	4.2	11	84	20
122	103.28	30.90	4.0	11	85	20
123	103.90	31.37	4.6	11	83	25

124	103.98	31.47	4.3	11	73	29
125	103.62	31.21	5.0	11	75	30
126	104.34	31.87	4.2	11	82	32
127	103.87	31.37	4.8	11	82	33
128	104.48	31.97	4.0	11	50	48
129	104.32	31.79	5.2	11	51	40
130	105.16	32.43	4.4	11	54	36
131	104.51	31.99	4.2	11	57	54
132	103.30	30.98	4.9	11	58	32
133	104.95	32.32	4.9	11	65	46
134	103.99	31.72	4.0	11	67	23
135	105.13	32.52	4.4	11	69	26
136	103.51	31.21	4.0	11	70	20
137	103.62	31.27	4.3	11	71	70
138	104.17	31.84	4.6	11	71	31
139	103.28	31.05	4.6	11	76	41
140	103.27	31.05	4.1	11	86	71
141	104.52	31.98	4.2	12	87	9
142	104.34	31.84	4.3	12	79	14
143	103.72	31.31	4.2	12	67	23
144	103.45	31.18	4.3	12	66	35
145	104.88	32.30	4.8	12	56	36
146	104.38	31.87	4.3	12	87	40
147	103.98	31.45	5.0	12	57	45
148	104.59	32.15	4.4	12	50	40
149	105.03	32.37	4.8	12	50	41
150	105.29	32.52	4.5	12	51	40
151	105.03	32.42	4.7	12	51	41
152	104.26	31.90	4.0	12	77	55
153	104.61	32.17	4.2	12	64	46
154	105.30	32.58	4.5	12	68	54
155	103.53	31.25	4.1	12	69	36
156	103.44	31.17	5.0	12	70	20
157	104.29	31.97	4.6	12	71	29
158	103.52	31.10	4.2	12	90	79
159	103.68	31.27	4.1	13	87	5
160	103.92	31.50	4.1	13	74	40
161	105.25	32.57	4.4	13	49	41
162	104.44	32.07	4.1	13	48	42
163	104.45	32.05	4.5	13	49	47
164	104.53	32.05	4.9	13	50	47
165	104.03	31.55	4.5	13	51	39
166	105.23	32.52	4.0	13	51	41
167	103.94	31.50	4.0	13	86	57

168	103.85	31.35	4.5	13	59	31
169	103.57	31.30	4.2	13	85	60
170	103.87	31.39	4.1	13	61	37
171	104.37	31.88	4.3	13	63	27
172	105.18	32.52	4.5	13	65	25
173	103.73	31.31	4.1	13	72	67
174	104.00	31.58	5.0	13	69	33
175	105.53	32.75	4.4	13	73	65
176	103.44	31.13	4.0	13	90	35
177	103.58	31.07	4.2	13	90	55
178	103.47	31.02	4.0	14	71	21
179	103.59	31.19	4.7	14	75	30
180	103.39	31.06	5.0	14	85	30
181	103.95	31.45	5.6	14	61	31
182	104.13	31.72	5.0	14	62	37
183	103.99	31.64	4.2	14	90	38
184	105.13	32.52	4.0	14	53	39
185	104.13	31.70	4.1	14	49	41
186	104.52	32.10	4.1	14	53	41
187	105.19	32.59	4.8	14	61	46
188	104.25	31.88	4.3	14	47	46
189	104.42	32.02	4.1	14	50	46
190	104.40	32.12	4.0	14	50	47
191	103.88	31.40	4.8	14	55	35
192	104.50	32.10	4.8	14	55	47
193	104.14	31.73	4.1	14	55	52
194	103.84	31.40	4.8	14	56	34
195	103.78	31.37	4.8	14	56	54
196	104.24	31.90	4.0	14	59	34
197	103.75	31.38	4.3	14	61	47
198	105.17	32.50	4.4	14	81	64
199	103.23	31.02	4.8	14	66	37
200	103.65	31.30	4.2	14	86	75
201	105.57	32.78	5.4	14	87	75
202	104.47	32.09	4.4	14	79	77
203	104.64	32.18	5.1	14	90	80
204	105.50	32.73	5.1	14	81	53
205	104.24	31.77	4.2	14	82	80
206	105.72	32.82	4.3	14	85	81
207	105.33	32.55	6.4	14	90	90
208	103.39	30.89	4.0	15	82	9
209	103.40	31.08	5.1	15	84	9
210	104.92	32.32	4.6	15	74	19
211	104.18	31.87	4.3	15	58	34

212	105.37	32.59	4.3	15	55	35
213	105.13	32.47	4.3	15	56	40
214	103.90	31.38	4.5	15	50	41
215	104.60	32.13	5.0	15	47	43
216	103.82	31.47	4.0	15	83	43
217	103.92	31.40	4.3	15	50	42
218	104.51	32.09	4.2	15	50	48
219	105.18	32.52	4.7	15	57	50
220	104.00	31.60	4.0	15	52	38
221	104.12	31.78	4.6	15	52	41
222	103.80	31.40	4.1	15	56	36
223	104.13	31.80	4.3	15	59	32
224	103.86	31.39	4.5	15	63	28
225	104.12	31.60	4.5	15	64	62
226	103.72	31.35	4.5	15	65	42
227	103.52	31.25	4.7	15	90	65
228	105.60	32.78	5.7	15	76	69
229	103.77	31.43	4.2	15	71	40
230	105.40	32.60	4.5	15	76	72
231	103.83	31.52	4.1	15	74	61
232	105.60	32.75	4.6	15	90	82
233	103.53	31.18	4.0	16	77	16
234	105.18	32.53	4.1	16	83	24
235	104.94	32.31	4.0	16	67	25
236	104.08	31.78	4.1	16	66	26
237	103.83	31.45	4.8	16	62	29
238	104.06	31.83	4.5	16	67	37
239	103.73	31.39	4.0	16	52	41
240	105.03	32.40	4.0	16	47	43
241	103.66	31.31	4.3	16	46	44
242	103.49	31.17	5.0	16	46	44
243	104.02	31.68	4.1	16	45	45
244	104.76	32.23	4.6	16	61	45
245	104.20	31.78	4.0	16	90	47
246	104.12	31.83	4.3	16	48	43
247	104.18	31.87	4.9	16	55	46
248	105.00	32.37	5.0	16	59	31
249	103.28	31.09	4.1	16	75	52
250	105.08	32.40	4.7	16	80	45
251	103.77	31.38	4.5	16	81	69
252	103.95	31.59	5.0	17	81	10
253	103.72	31.35	5.0	17	66	26
254	105.22	32.58	4.7	17	77	26
255	104.22	31.92	4.7	17	68	29

256	103.32	31.10	4.0	17	53	37
257	103.84	31.45	5.7	17	52	38
258	104.08	31.70	5.1	17	51	39
259	104.40	32.10	4.2	17	47	43
260	103.59	31.29	4.2	17	46	44
261	103.64	31.30	4.1	17	46	45
262	103.92	31.43	5.1	17	47	46
263	104.98	32.37	4.7	17	47	46
264	105.07	32.42	4.1	17	48	42
265	105.23	32.55	5.4	17	48	43
266	105.27	32.55	4.0	17	73	54
267	104.12	31.82	4.2	17	55	38
268	103.82	31.41	4.2	17	72	67
269	104.98	32.31	4.6	17	68	27
270	103.57	31.23	4.7	17	74	27
271	105.50	32.90	4.0	17	79	79
272	104.62	32.13	4.7	17	81	44
273	103.50	31.20	4.7	18	66	24
274	104.08	31.73	4.3	18	51	40
275	104.92	32.40	4.2	18	78	68
276	104.00	31.63	4.5	19	72	18